

A Novel Vector-Field-Based Motion Planning for 3D Nonholonomic Robots

Xiaodong He, Zhiyong Sun and Zhongkui Li

Abstract—This paper focuses on the motion planning for mobile robots in 3D, which are modelled by 6-DOF rigid body systems with nonholonomic constraints. We not only specify the target position, but also bring in the requirement of the heading direction at the terminal time, which gives rise to a new and more challenging 3D motion planning problem. The proposed planning algorithm involves a novel velocity vector field (VF) over the workspace, and by following the VF, the robot can be navigated to the destination with the specified heading direction. In order to circumvent potential collisions with obstacles and other robots, a composite VF is presented by composing the navigation VF and an additional VF tangential to the boundary of the dangerous area. Moreover, we propose a priority-based algorithm to deal with the motion coupling among multiple robots. Finally, numerical simulations are conducted to verify the theoretical results.

Index Terms—Motion planning, nonholonomic constraint, vector field, obstacle avoidance, collision avoidance.

I. INTRODUCTION

As a fundamental problem in robotics and control, motion planning refers to finding a path or trajectory which guides robots from an initial position to a goal position, without collisions of obstacles or other robots. Basically, motion planning has been employed in a wide range of robotic systems, e.g., planar mobile robots [1], [2], [3], marine vessels [4], [5], [6], and quadrotors [7], [8], [9]. Generally, for the purpose of weight and cost reduction, robotic systems are designed with fewer actuators than degrees of freedom (DOF), resulting in underactuated systems. From the kinematic level of mobile robots in 3D, a typical form of underactuation is that the robot modelled by a 6-DOF rigid body has no sway and heave velocity, while only one surge velocity and three angular velocities serve as control inputs. Such a system model is referred to as a 3D nonholonomic rigid body, and can be utilized to describe the kinematics of various robotic systems such as fixed-wing UAVs [10], [11], [12], [13] and autonomous underwater vehicles [14], [15], [16], [17].

Essentially, the motion model of a 3D nonholonomic mobile robot can be described by a nonholonomic constrained rigid body with six DOFs. Resulting from the nonholonomic

constraints, the heading direction of the robot is restricted and always points to the x -axis of the body-fixed frame [18]. Thus, we are motivated to take into account not only goal position but also heading direction of the robot in motion planning. For instance, in real-world scenarios, the heading directions of multiple missiles are typically specified in the terminal guidance so as to realize a better performance of coordinated attack. Similarly, in surveillance tasks performed by multi-UAV systems, the final orientation of each UAV should point to a certain direction so as to obtain the largest overall surveillance area. Therefore, from the perspectives of theory and practice, it is of great importance to investigate the motion planning with specified position and heading direction.

However, it is not trivial to simultaneously plan the position and heading direction of 3D nonholonomic robots, and the main challenge arises from the underactuation caused by the nonholonomic constraints. On one hand, since the linear velocity is restricted to the heading direction, we should adjust the heading direction to point towards the direction to destination such that the robot can move towards the goal position. On the other hand, the heading direction is not only employed for reaching the destination, but also has to satisfy the requirement of terminal direction, which demonstrates the underactuated characteristics of 3D nonholonomic robots. Besides, compared to the 2D case which has only one rotational DOF, the rotation control in 3D is more complicated due to the coupling among three different rotational DOFs, leading to a more challenging motion planning problem.

In the literature, there exist several commonly-used methodologies for motion planning, including the roadmap method [19], [20], [21], the cell decomposition approach [22], [23], [24], the sampling-based algorithm [25], [26], [27], and so on. But these methods cannot be directly applied to the nonholonomic robotic systems. Although certain optimization-based algorithms can handle the nonholonomic constraints, such as [28], [29], [30], [31], [32], [33], the feasibility of the optimization problem cannot be guaranteed or it suffers from heavy computational burden once the nonholonomic constraints are taken into consideration. Besides, the control inputs derived from these optimization-based algorithms are open-loop, relying only on time, thereby not robust to disturbances.

To overcome the above-mentioned limitations, we utilize the vector field (VF) method to solve the motion planning problem for the 3D nonholonomic robots. Specifically, a velocity VF is defined over the workspace and the integral curve of the VF converges to the goal point. Compared to the optimization-based method, the VF motion planning specifies a reactive feedback in the sense that it is only related to the current state

This work was supported by the National Natural Science Foundation of China (61973006, T2121002), and the China Postdoctoral Science Foundation (2022M720242). (*Corresponding author: Zhongkui Li.*)

X. He and Z. Li are with the State Key Laboratory for Turbulence and Complex Systems, Department of Mechanics and Engineering Science, College of Engineering, Peking University, Beijing 100871, China (e-mail: hxdupc@pku.edu.cn; zhongkli@pku.edu.cn)

Z. Sun is with the Department of Electrical Engineering, Eindhoven University of Technology, 5612 AZ Eindhoven, The Netherlands (sun.zhiyong.cn@gmail.com)

while the stage of replanning is not involved. Furthermore, the VF directly specifies the heading direction at each point, which provides a reference to tune the attitude of the robot so as to follow such a heading direction. In this way, the challenge caused by the nonholonomic constraints can be suitably handled via the VF method. Although several works have employed VF in the motion planning problem, such as [34], [35], [36], [37], [38], [39], most of them focus on particle agents in 2D instead of rigid bodies in 3D. Additionally, the heading direction of the nonholonomic robot is rarely considered in the existing VF-based motion planning results.

Therefore, in this paper, we investigate the motion planning problem of 3D nonholonomic robots via the VF method, where the terminal heading direction is taken into account. Moreover, the robot is modelled by a 6-DOF nonholonomic constrained rigid body rather than a particle agent. The contributions of this paper are given below.

- 1) Concerning the nonholonomic robot moving in an obstacle-free environment, we design a navigation VF (N-VF) which converges to any expected target position. More importantly, the N-VF points to a specified direction at the destination. Thus, by moving along the N-VF, the nonholonomic robot can reach the target position with the specified heading direction.
- 2) An obstacle avoidance VF (OA-VF) is proposed for motion planning in an obstacle-cluttered environment. The shape of the obstacle is not restricted as long as it has a convex surface described by an implicit function, and the obstacle can be either static or moving. The OA-VF is composed of the N-VF and an additional VF tangential to the obstacle surface, and the composite OA-VF is free of any singularity.
- 3) For motion planning of multiple nonholonomic robots, a collision avoidance VF (CA-VF) is proposed to evade the collisions among nonholonomic robots. In order to reduce the motion coupling in collision avoidance, we propose a priority-based algorithm where the movement of higher prioritized nonholonomic robots is independent of the lower ones, so as to achieve the motion decoupling.
- 4) To apply the proposed VF to the 3D rigid body, we design another two auxiliary VFs which are always orthogonal to the N/OA/CA-VF. Moreover, such two auxiliary VFs are also orthogonal to each other. Therefore, these three VFs construct the basis of a body-fixed frame in \mathbb{R}^3 , which can be further utilized as reference in the attitude control of 3-D nonholonomic robots.

To the best of our knowledge, it is the first time that the motion planning problem of 6-DOF nonholonomic rigid-body robots in 3D is investigated under the consideration of both specified terminal positions and heading directions.

This paper is organized as follows. Section II provides the preliminaries and formulates the problems. The motion planning algorithms in obstacle-free and obstacle-cluttered environments are proposed in Section III and Section IV, respectively. Section V provides the cooperative motion planning algorithm of multiple nonholonomic robots. Numerical simu-

lation results are given in Section VI, followed by Section VII concluding the whole paper.

II. PRELIMINARIES AND PROBLEM FORMULATION

In this paper, the nonholonomic robot is modelled by a 6-DOF rigid body moving in the 3D Euclidean space \mathbb{R}^3 . Let \mathcal{F}_e denote the earth-fixed frame and let \mathcal{F}_b denote the body-fixed frame, which is attached to the center of mass of the robot. The position of the nonholonomic robot in \mathcal{F}_e is described by a vector $\mathbf{p} = [x \ y \ z]^T$, while the attitude is specified by a rotation matrix \mathbf{R} , which depicts the rotation of \mathcal{F}_b relative to \mathcal{F}_e . The nonholonomic robot's angular velocity and linear velocity are denoted by $\boldsymbol{\Omega} = [\Omega_x \ \Omega_y \ \Omega_z]^T \in \mathbb{R}^3$ and $\mathbf{v} = [v_x \ v_y \ v_z]^T \in \mathbb{R}^3$, respectively, which are both provided in the body-fixed frame \mathcal{F}_b . For $\forall \mathbf{a} = [a_x \ a_y \ a_z]^T \in \mathbb{R}^3$, we define the linear map “ \wedge ” as follows

$$\mathbf{a}^\wedge = \begin{bmatrix} 0 & -a_z & a_y \\ a_z & 0 & -a_x \\ -a_y & a_x & 0 \end{bmatrix}. \quad (1)$$

Then, for $\forall \mathbf{a}, \mathbf{b} \in \mathbb{R}^3$, there holds $\mathbf{a}^\wedge \mathbf{b} = \mathbf{a} \times \mathbf{b}$, where “ \times ” denotes the cross product. Thus, the kinematics of the nonholonomic robot can be given by

$$\dot{\mathbf{R}} = \mathbf{R}\boldsymbol{\Omega}^\wedge, \quad (2a)$$

$$\dot{\mathbf{p}} = \mathbf{R}\mathbf{v}, \quad (2b)$$

which describes the rotation and translation kinematics, respectively. Note that the motion of the nonholonomic robot is restricted by the nonholonomic constraints, so that the linear velocities along the y -axis and z -axis of the body-fixed frame \mathcal{F}_b are both zero, that is, $v_y = v_z = 0$. Hence, the nonholonomic robot with 6 DOFs is controlled by only 4 inputs, i.e., $\Omega_x, \Omega_y, \Omega_z, v_x$, demonstrating that the nonholonomic robot is a typical underactuated system.

Problem Formulation: Consider a swarm of nonholonomic robots labelled by $i \in \{1, \dots, N\}$, and the kinematics of each robot is described by (2). Let \mathbf{p}_{d_i} denote a target position and let \mathbf{e}_{d_i} denote a desired vector direction. Then, we design the angular velocity $\boldsymbol{\Omega}_i^\wedge$ and the linear velocity \mathbf{v}_i such that

- 1) the i -th nonholonomic robot is driven to the target \mathbf{p}_{d_i} , and in the meantime, the heading direction points along the desired direction \mathbf{e}_{d_i} ;
- 2) the i -th nonholonomic robot does not collide with the obstacles located in the environment;
- 3) the i -th nonholonomic robot does not collide with any other nonholonomic robots in the swarm.

III. MOTION PLANNING IN OBSTACLE-FREE ENVIRONMENTS

This section considers the motion planning of a single nonholonomic robot in an obstacle-free environment. We firstly design the VF which guides the motion of the nonholonomic robot to the target position and desired heading direction, and then derive the controller based on the proposed VF.

A. Vector Field Design

Before designing the VF, we provide the notation of coordinate frames. The 3D earth-fixed frame \mathcal{F}_e is commonly described by the orthogonal coordinates (x, y, z) . Actually, \mathcal{F}_e can also be formulated under the cylindrical coordinates or spherical coordinates. In the following, we let $\mathcal{F}_{\alpha\beta\gamma}$ represent the earth-fixed frame given by the coordinates (α, β, γ) . For example, \mathcal{F}_{xyz} denotes the 3D orthogonal coordinate frame. Then, we design the following N-VF to guide the nonholonomic robot to the target position with the specified heading direction.

Theorem 1. *Let e_x, e_y, e_z denote the basis of the coordinate frame \mathcal{F}_{xyz} . Define the navigation vector field (N-VF)*

$$\mathbf{F} = F_x e_x + F_y e_y + F_z e_z, \quad (3)$$

where the components are

$$F_x = x^2 - y^2 - z^2, \quad (4a)$$

$$F_y = 2xy, \quad (4b)$$

$$F_z = 2xz. \quad (4c)$$

Then, the following properties hold.

- 1) \mathbf{F} always lies in the plane $\Sigma : ay + bz = 0$, where a, b are arbitrary constants in \mathbb{R} .
- 2) The integral curve of \mathbf{F} passes through the origin of \mathcal{F}_{xyz} , and the tangential vector at the origin points along the direction of the x -axis.

Proof. 1) Consider a new coordinate frame $\mathcal{F}_{xr\theta}$, and the coordinate transformation between \mathcal{F}_{xyz} and $\mathcal{F}_{xr\theta}$ is defined by

$$x = x, \quad y = r \cos \theta, \quad z = r \sin \theta. \quad (5)$$

Thus, the N-VF components in (4) can be written as

$$F_x = x^2 - r^2, \quad F_y = 2xr \cos \theta, \quad F_z = 2xz \sin \theta. \quad (6)$$

Let e_x, e_r, e_θ denote the basis of the coordinate frame $\mathcal{F}_{xr\theta}$, and then the transformation between $\{e_x, e_y, e_z\}$ and $\{e_x, e_r, e_\theta\}$ can be given by

$$\begin{bmatrix} e_x \\ e_y \\ e_z \end{bmatrix} = \begin{bmatrix} 1 & 0 & 0 \\ 0 & \cos \theta & -\sin \theta \\ 0 & \sin \theta & \cos \theta \end{bmatrix} \begin{bmatrix} e_x \\ e_r \\ e_\theta \end{bmatrix}. \quad (7)$$

Substituting (6) and (7) into (3), and after computation, the N-VF \mathbf{F} can be expressed in the coordinate frame $\mathcal{F}_{xr\theta}$ as

$$\mathbf{F} = F_x e_x + F_r e_r + F_\theta e_\theta, \quad (8)$$

where the components are

$$F_x = x^2 - r^2, \quad F_r = 2xr, \quad F_\theta = 0. \quad (9)$$

Regarding the plane $\Sigma : ay + bz = 0$, it can be reformulated in the coordinate frame $\mathcal{F}_{xr\theta}$ as $\Sigma : r(a \cos \theta + b \sin \theta) = 0$. Due to $r \neq 0$, the plane Σ can be further simplified to be

$$\Sigma : \theta - \theta_0 = 0, \quad (10)$$

where θ_0 is a constant defined by $\theta_0 = \text{atan2}(-a, b)$. Thus, the normal vector of the plane Σ in the coordinate frame $\mathcal{F}_{xr\theta}$ can be given by $\mathbf{n}_\Sigma = e_\theta$. We compute the dot product of the

normal vector \mathbf{n}_Σ and the N-VF \mathbf{F} provided in (8), and it is obtained that

$$\mathbf{n}_\Sigma \cdot \mathbf{F} = 0, \quad (11)$$

which indicates \mathbf{F} is perpendicular to the normal vector of the plane Σ . That is to say, \mathbf{F} always lies in the plane Σ .

2) Having proved that the N-VF \mathbf{F} is in the plane Σ , we will then calculate the integral curve of \mathbf{F} in Σ . For simplicity, another coordinate transformation is made for \mathbf{F} on the basis of $\mathcal{F}_{xr\theta}$. Define a new coordinate frame $\mathcal{F}_{\rho\varphi\theta}$, and the transformation between $\mathcal{F}_{xr\theta}$ and $\mathcal{F}_{\rho\varphi\theta}$ is

$$x = \rho \cos \varphi, \quad r = \rho \sin \varphi, \quad \theta = \theta. \quad (12)$$

Then, the N-VF components in (9) can be expressed as

$$F_x = \rho^2 (\cos^2 \varphi - \sin^2 \varphi), \quad F_r = 2\rho^2 \cos \varphi \sin \varphi, \quad F_\theta = 0. \quad (13)$$

The basis of the coordinate frame $\mathcal{F}_{\rho\varphi\theta}$ is denoted by $e_\rho, e_\varphi, e_\theta$, and the transformation between $\{e_x, e_r, e_\theta\}$ and $\{e_\rho, e_\varphi, e_\theta\}$ is

$$\begin{bmatrix} e_x \\ e_r \\ e_\theta \end{bmatrix} = \begin{bmatrix} \cos \varphi & -\sin \varphi & 0 \\ \sin \varphi & \cos \varphi & 0 \\ 0 & 0 & 1 \end{bmatrix} \begin{bmatrix} e_\rho \\ e_\varphi \\ e_\theta \end{bmatrix}. \quad (14)$$

By substituting (13) and (14) into (8), the N-VF \mathbf{F} can be provided in $\mathcal{F}_{xr\theta}$ as

$$\mathbf{F} = F_\rho e_\rho + F_\varphi e_\varphi + F_\theta e_\theta, \quad (15)$$

where the components are

$$F_\rho = \rho^2 \cos \varphi, \quad F_r = \rho^2 \sin \varphi, \quad F_\theta = 0. \quad (16)$$

Owing to $F_\theta = 0$, we can compute the integral curve of \mathbf{F} in the plane $\Sigma : \theta - \theta_0 = 0$ based on the VF components F_ρ and F_φ . In Σ , the integral curve of \mathbf{F} is the solution of the following ordinary differential equations

$$\frac{d\rho}{dt} = F_\rho, \quad \rho \frac{d\varphi}{dt} = F_\varphi. \quad (17)$$

Then, it can be derived that

$$\frac{d\rho}{\rho d\varphi} = \frac{F_\rho}{F_\varphi} = \frac{\cos \varphi}{\sin \varphi}, \quad (18)$$

where (16) is utilized, and it follows that

$$\frac{1}{\rho} d\rho = \cot \varphi d\varphi. \quad (19)$$

By integrating (19), we can obtain that

$$\rho = C \sin \varphi, \quad (20)$$

where $C \in \mathbb{R}$ is a constant. It should be mentioned that (20) represents a surface rather than a curve in the coordinate frame $\mathcal{F}_{\rho\varphi\theta}$. Let Λ denote the surface given in (20), and by coordinate transformations (5) and (12), it can be expressed in the coordinate frame \mathcal{F}_{xyz} as

$$\Lambda : x^2 + y^2 + z^2 - C\sqrt{y^2 + z^2} = 0. \quad (21)$$

Since it has been proved that the N-VF \mathbf{F} lies in the plane Σ , then the integral curve of \mathbf{F} , denoted by ξ , can be given by

$$\xi : \begin{cases} x^2 + y^2 + z^2 - C\sqrt{y^2 + z^2} = 0 \\ -\sin \theta_0 y + \cos \theta_0 z = 0 \end{cases}, \quad (22)$$

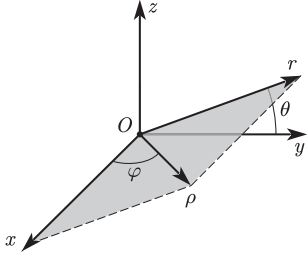


Fig. 1. Illustrations of coordinate frames \mathcal{F}_{xyz} , $\mathcal{F}_{xr\theta}$, $\mathcal{F}_{\rho\varphi\theta}$.

where θ_0 is the constant defined in (10). By substituting $(x, y, z) = (0, 0, 0)$ into (22), it is easily verified that the integral curve ξ passes through the origin.

Furthermore, we can compute the tangential vector of ξ based on the formulation in (22). Since ξ is defined as the intersection of two surfaces, the tangential vector can be given by the cross product of the normal vectors of two surfaces. Define $f_1 = x^2 + y^2 + z^2 - C\sqrt{y^2 + z^2}$ and $f_2 = -\sin\theta_0 y + \cos\theta_0 z$, and then the normal vectors of Λ and Σ are given by

$$\begin{aligned} \mathbf{n}_\Lambda &= \frac{\partial f_1}{\partial x} \mathbf{e}_x + \frac{\partial f_1}{\partial y} \mathbf{e}_y + \frac{\partial f_1}{\partial z} \mathbf{e}_z \\ &= 2x\mathbf{e}_x + \left(2y - \frac{Cy}{\sqrt{y^2 + z^2}}\right) \mathbf{e}_y + \left(2z - \frac{Cz}{\sqrt{y^2 + z^2}}\right) \mathbf{e}_z, \\ \mathbf{n}_\Sigma &= \frac{\partial f_2}{\partial x} \mathbf{e}_x + \frac{\partial f_2}{\partial y} \mathbf{e}_y + \frac{\partial f_2}{\partial z} \mathbf{e}_z \\ &= -\sin\theta_0 \mathbf{e}_y + \cos\theta_0 \mathbf{e}_z \\ &= -\frac{z}{\sqrt{y^2 + z^2}} \mathbf{e}_y + \frac{y}{\sqrt{y^2 + z^2}} \mathbf{e}_z. \end{aligned}$$

Having obtained \mathbf{n}_Λ and \mathbf{n}_Σ , we can calculate the tangential vector of the integral curve ξ as

$$\begin{aligned} \boldsymbol{\tau}_\xi &= \mathbf{n}_\Sigma \times \mathbf{n}_\Lambda \\ &= \left(C - 2\sqrt{y^2 + z^2}\right) \mathbf{e}_x + \frac{2xy}{\sqrt{y^2 + z^2}} \mathbf{e}_y + \frac{2xz}{\sqrt{y^2 + z^2}} \mathbf{e}_z \end{aligned}$$

Due to the property of

$$\lim_{x,y,z \rightarrow 0} \frac{2xy}{\sqrt{y^2 + z^2}} = 0, \quad \lim_{x,y,z \rightarrow 0} \frac{2xz}{\sqrt{y^2 + z^2}} = 0,$$

the tangential vector $\boldsymbol{\tau}_\xi$ at the origin of the coordinate frame \mathcal{F}_{xyz} can be obtained as

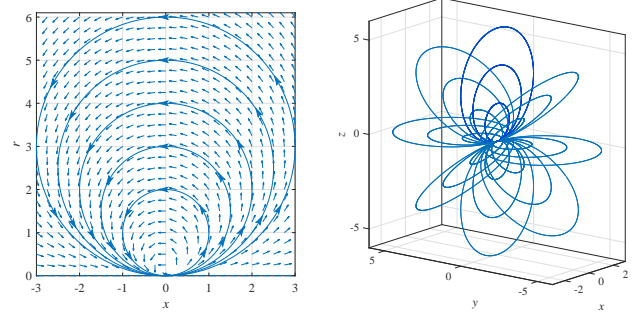
$$\boldsymbol{\tau}_\xi|_{(x,y,z)=(0,0,0)} = C\mathbf{e}_x, \quad (23)$$

which indicates that the tangential vector $\boldsymbol{\tau}_\xi$ at the origin of \mathcal{F}_{xyz} points along the x -axis. \square

Remark 1. The coordinate frames \mathcal{F}_{xyz} , $\mathcal{F}_{xr\theta}$, $\mathcal{F}_{\rho\varphi\theta}$ are all earth-fixed frames, and the relations between these three frames are intuitively illustrated in Fig. 1. The coordinate frame $\mathcal{F}_{xr\theta}$ actually defines a plane which passes through the x -axis and forms an angle of θ with respect to the y -axis. Based on $\mathcal{F}_{xr\theta}$, the coordinate frame $\mathcal{F}_{\rho\varphi\theta}$ further provides the polar coordinates (ρ, φ) in the xOr plane.

Remark 2. It is indicated by Theorem 1 that the integral curve of the N-VF \mathbf{F} always lies in the xOr plane, which

is expressed as (20) in the polar coordinates (ρ, φ) . By substituting (12) into (20), we can obtain the expression of the integral curve in orthogonal coordinates (x, r) , that is, $x^2 + (r - \frac{C}{2})^2 = (\frac{C}{2})^2$. This demonstrates that the integral curves in the xOr plane are circles located at $(x, r) = (0, \frac{C}{2})$ with radius $|\frac{C}{2}|$. Fig. 2(a) illustrates the N-VF \mathbf{F} and its integral curve with $C > 0$ in the xOr plane. Once rotating the xOr plane around the x -axis, which is equivalent to choosing different values of θ , we can obtain the integral curves of \mathbf{F} in the overall 3D space, as shown in Fig. 2(b).



(a) Vector field in xOr plane.

(b) Integral curves of vector field.

Fig. 2. Navigation vector field \mathbf{F} and its integral curves.

Theorem 1 can be extended to arbitrary goal position and goal orientation, which is given in the following corollary.

Corollary 1. Let $\mathbf{p}_d = [x_d \ y_d \ z_d]^T$ denote a desired position and $\mathbf{e}_d = \mathbf{R}_d \mathbf{e}_x$ a desired direction, where \mathbf{R}_d represents the rotation relative to the coordinate frame \mathcal{F}_{xyz} . Define the following N-VF

$$\tilde{\mathbf{F}} = \tilde{F}_x \mathbf{R}_d^T \mathbf{e}_x + \tilde{F}_y \mathbf{R}_d^T \mathbf{e}_y + \tilde{F}_z \mathbf{R}_d^T \mathbf{e}_z, \quad (24)$$

where the components are

$$\tilde{F}_x = (x - x_d)^2 - (y - y_d)^2 - (z - z_d)^2, \quad (25a)$$

$$\tilde{F}_y = 2(x - x_d)(y - y_d), \quad (25b)$$

$$\tilde{F}_z = 2(x - x_d)(z - z_d). \quad (25c)$$

Then, the N-VF $\tilde{\mathbf{F}}$ passes through the position \mathbf{p}_d and points along the direction of \mathbf{e}_d simultaneously.

B. Controller Design

Theorem 1 provides a VF which passes through a point with a desired direction. This naturally inspires us that we can make the nonholonomic robot to follow the direction of the VF, so that it will be able to arrive at the goal point with a specified heading direction. Note that the nonholonomic robot is a 3D rigid body, and its heading direction is actually the x -axis direction of the body-fixed frame \mathcal{F}_b . Although the VF in Theorem 1 provides the x -axis direction of \mathcal{F}_b , the directions of y -axis and z -axis are undetermined yet, leading to the result that the angular velocity Ω^\wedge of the nonholonomic robot cannot be derived either.

Hence, in the following, we design two extra VFs which represents the y -axis and z -axis directions of the body-fixed frame \mathcal{F}_b , and then plus the N-VF \mathbf{F} in Theorem 1, an

auxiliary attitude matrix \mathbf{R}_a can be constructed based on these three VFs. By tracking the attitude \mathbf{R}_a with an angular velocity controller, the nonholonomic robot can align its heading direction with the N-VF \mathbf{F} , so as to accomplish the task of motion planning.

Lemma 1. Define a VF \mathbf{G} as follows

$$\mathbf{G} = G_x \mathbf{e}_x + G_y \mathbf{e}_y + G_z \mathbf{e}_z, \quad (26)$$

where the components are

$$G_x = 2x\sqrt{y^2 + z^2}, \quad (27a)$$

$$G_y = (y^2 + z^2 - x^2) \frac{y}{\sqrt{y^2 + z^2}}, \quad (27b)$$

$$G_z = (y^2 + z^2 - x^2) \frac{z}{\sqrt{y^2 + z^2}}. \quad (27c)$$

Then, \mathbf{G} is in the xOz plane and orthogonal to the N-VF \mathbf{F} .

Proof. By substituting the coordinate transformation (5) and basis transformation (7) into (26) and (27), \mathbf{G} can be rewritten in the frame $\mathcal{F}_{x\theta}$ as

$$\mathbf{G} = G_x \mathbf{e}_x + G_r \mathbf{e}_r + G_\theta \mathbf{e}_\theta, \quad (28)$$

where the components are

$$G_x = 2xr, \quad G_r = r^2 - x^2, \quad G_\theta = 0. \quad (29)$$

As illustrated in the proof of Theorem 1, $G_\theta = 0$ demonstrates that \mathbf{G} lies in the xOr plane. To prove the orthogonality, we compute the dot product of \mathbf{F} and \mathbf{G} , which is given by

$$\mathbf{F} \cdot \mathbf{G} = F_x G_x + F_r G_r + F_\theta G_\theta \quad (30)$$

Substituting (9) and (29) into (30), we have

$$\mathbf{F} \cdot \mathbf{G} = 0, \quad (31)$$

which implies the VFs \mathbf{F} and \mathbf{G} are orthogonal. \square

Based on \mathbf{F} and \mathbf{G} , we define another VF \mathbf{H} by the cross product of \mathbf{F} and \mathbf{G} , that is

$$\mathbf{H} = \mathbf{G} \times \mathbf{F} = H_x \mathbf{e}_x + H_y \mathbf{e}_y + H_z \mathbf{e}_z, \quad (32)$$

where

$$H_x = 0, \quad (33a)$$

$$H_y = -(x^2 + y^2 + z^2) \frac{z}{\sqrt{y^2 + z^2}}, \quad (33b)$$

$$H_z = (x^2 + y^2 + z^2) \frac{y}{\sqrt{y^2 + z^2}}. \quad (33c)$$

Therefore, it follows from (31) and (32) that each two VFs of $\mathbf{F}, \mathbf{G}, \mathbf{H}$ are orthogonal, which indeed defines a 3D Cartesian coordinate frame at every point (x, y, z) in \mathbb{R}^3 . Then, an attitude matrix \mathbf{R}_a can be constructed to describe the attitude of such a coordinate frame. For simplicity, let vectors $\zeta_X, \zeta_Y, \zeta_Z$ denote the components of $\mathbf{F}, \mathbf{H}, \mathbf{G}$ at each point, and then it follows that

$$\zeta_X = \begin{bmatrix} F_x \\ F_y \\ F_z \end{bmatrix}, \quad \zeta_Y = \begin{bmatrix} H_x \\ H_y \\ H_z \end{bmatrix}, \quad \zeta_Z = \begin{bmatrix} G_x \\ G_y \\ G_z \end{bmatrix}, \quad (34)$$

where the components are given in (4)(33)(27), respectively. Note that the vectors $\zeta_X, \zeta_Y, \zeta_Z$ are orthogonal to each other, based on which we can define the following auxiliary attitude matrix

$$\mathbf{R}_a = \begin{bmatrix} \frac{\zeta_X}{\|\zeta_X\|} & \frac{\zeta_Y}{\|\zeta_Y\|} & \frac{\zeta_Z}{\|\zeta_Z\|} \end{bmatrix}. \quad (35)$$

It can be observed from (4) that the N-VF \mathbf{F} is singular, that is, $F_x = F_y = F_z = 0$, only at the origin (the goal point). Thus, the auxiliary attitude matrix \mathbf{R}_a is well defined almost everywhere except for the destination. The time derivative of \mathbf{R}_a is

$$\dot{\mathbf{R}}_a = \begin{bmatrix} \frac{d}{dt} \left(\frac{\zeta_X}{\|\zeta_X\|} \right) & \frac{d}{dt} \left(\frac{\zeta_Y}{\|\zeta_Y\|} \right) & \frac{d}{dt} \left(\frac{\zeta_Z}{\|\zeta_Z\|} \right) \end{bmatrix}, \quad (36)$$

where

$$\frac{d}{dt} \left(\frac{\zeta_*}{\|\zeta_*\|} \right) = \frac{\dot{\zeta}_*}{\|\zeta_*\|} - (\zeta_*^T \dot{\zeta}_*) \frac{\zeta_*}{\|\zeta_*\|^3}.$$

Lemma 2. The nonholonomic robot's heading direction is aligned with the N-VF \mathbf{F} if the nonholonomic robot's attitude \mathbf{R} tracks the auxiliary attitude \mathbf{R}_a .

Proof. Since each pair of the vectors $\zeta_X, \zeta_Y, \zeta_Z$ are orthogonal, the auxiliary attitude \mathbf{R}_a actually represents the attitude of a 3D coordinate frame. According to the construction in (35), the unit vectors along the x, y, z -axis of such a coordinate frame are given by $\frac{\zeta_X}{\|\zeta_X\|}, \frac{\zeta_Y}{\|\zeta_Y\|}, \frac{\zeta_Z}{\|\zeta_Z\|}$, respectively. Thus, once the nonholonomic robot tracks the auxiliary attitude \mathbf{R}_a , its heading direction will be aligned with the vector ζ_X , which is indeed the direction of the N-VF \mathbf{F} according to (34). \square

It is evident from Theorem 1 that the nonholonomic robot will arrive at the goal point with the desired heading direction if it moves along the N-VF \mathbf{F} , which is further converted by Lemma 2 to the attitude tracking of \mathbf{R} with respect to \mathbf{R}_a . In other words, once the nonholonomic robot tracks the attitude matrix \mathbf{R} , it can follow the N-VF \mathbf{F} to reach the goal point. Therefore, in the following, we will propose the control inputs of motion planning by solving the problem of attitude tracking.

Lemma 3. The nonholonomic robot's attitude \mathbf{R} tracks the auxiliary attitude \mathbf{R}_a under the angular velocity control law given below

$$\Omega^\wedge = -k_w \log_{\text{SO}(3)}(\mathbf{R}_a^{-1} \mathbf{R}) + \mathbf{R}^{-1} \dot{\mathbf{R}}_a \mathbf{R}_a^{-1} \mathbf{R}, \quad (37)$$

where $k_w > 0$ is the scalar control gain, and $\log_{\text{SO}(3)}$ is the logarithmic map in the Lie group $\text{SO}(3)$.

Proof. Define the attitude tracking error $\mathbf{R}_e = \mathbf{R}_a^{-1} \mathbf{R}$, and the time derivative of \mathbf{R}_e is

$$\dot{\mathbf{R}}_e = -\mathbf{R}_a^{-1} \dot{\mathbf{R}}_a \mathbf{R}_a^{-1} \mathbf{R} + \mathbf{R}_a^{-1} \dot{\mathbf{R}} \quad (38)$$

$$= \mathbf{R}_e (\Omega^\wedge - \mathbf{R}^{-1} \dot{\mathbf{R}}_a \mathbf{R}_a^{-1}), \quad (39)$$

where the rotation kinematics of the nonholonomic robot is employed. Let Ω_e^\wedge denote the velocity of the error system, that is

$$\Omega_e^\wedge = \Omega^\wedge - \mathbf{R}^{-1} \dot{\mathbf{R}}_a \mathbf{R}_a^{-1}. \quad (40)$$

Then, the error dynamics can be described by

$$\dot{\mathbf{R}}_e = \mathbf{R}_e \Omega_e^\wedge. \quad (41)$$

Based on the definition of \mathbf{R}_e , if there holds $\mathbf{R}_e = \mathbf{I}$, where \mathbf{I} is the identity matrix, then it is obtained that $\mathbf{R} = \mathbf{R}_a$, indicating the mission of attitude tracking is achieved. It has been proposed in [40] that regarding the system $\dot{\mathbf{R}} = \mathbf{R}\Omega^\wedge$ in the Lie group $\text{SO}(3)$, the control law $\Omega^\wedge = -k_w \log_{\text{SO}(3)}(\mathbf{R})$ exponentially stabilizes the state \mathbf{R} to \mathbf{I} . Hence, for the purpose of attitude tracking, the error system's velocity Ω_e^\wedge can be designed as

$$\Omega_e^\wedge = -k_w \log_{\text{SO}(3)}(\mathbf{R}_e), \quad (42)$$

which is able to realize $\mathbf{R}_e \rightarrow \mathbf{I}$. By substituting (42) into (40), we obtain the angular velocity controller of the nonholonomic robot as given in (37). \square

Regarding the control law of the linear velocity v_x , it can be straightforwardly chosen as a positive constant \bar{v} . When far away from the target, it is reasonable to provide the nonholonomic robot with a fairly large velocity, so that the distance error to the desired position (i.e., the origin of the earth-fixed frame) is introduced to the linear velocity additionally, implying that v_x is finally given by

$$v_x = k_v \|\mathbf{p}\| + \bar{v}. \quad (43)$$

To summarize, the control law for nonholonomic robot motion planning is presented in the following theorem.

Theorem 2. *The control laws (37) and (43) drive the nonholonomic robot moving to the origin of the earth-fixed frame \mathcal{F}_e along the N-VF \mathbf{F} , with the heading direction pointing along the x -axis of \mathcal{F}_e .*

Proof. The proof is trivial based on Theorem 1, Lemma 2 and Lemma 3. \square

Remark 3. *Theorem 2 provides the control law in the case where the goal point is the origin and goal direction is the x -axis. Regarding arbitrary desired point and direction, Corollary 1 has provided the related N-VF $\tilde{\mathbf{F}}$. Then, the angular velocity in (37) can be correspondingly revised by reconstructing the auxiliary attitude matrix \mathbf{R}_a with the aid of $\tilde{\mathbf{F}}$ in (24). Besides, the linear velocity in (43) can also be reformulated to be $v_x = k_v \|\mathbf{p} - \mathbf{p}_d\| + \bar{v}$.*

Remark 4. *The formulation in (27) and (33) is merely one possible way to construct two auxiliary VFs \mathbf{G} and \mathbf{H} , which in fact represent the directions of y -, z -axis of the body-fixed frame \mathcal{F}_b . Since there only exists a requirement for the nonholonomic robot's heading direction (i.e., the direction of x -axis), the directions of y -, z -axis can be freely designed as long as they can form a set of basis in 3D Cartesian frame. Of course, it should be mentioned that the vector fields \mathbf{G} and \mathbf{H} presented in this paper have explicit geometric meanings. More specifically, \mathbf{G} represents the outward normal vector of the integral curves (i.e., the circles shown in Fig. 2(a)), while \mathbf{H} represents the normal vector of the xOy plane.*

IV. MOTION PLANNING IN OBSTACLE-CLUTTERED ENVIRONMENTS

In this section, we consider the motion planning of a nonholonomic robot in an obstacle-cluttered environment. In

advance of designing planning algorithms, the obstacles should be established mathematically.

Consider a continuous function $\Upsilon(\mathbf{p}; \mathbf{p}_o) : \mathbb{R}^3 \rightarrow \mathbb{R}$, where $\mathbf{p} = [x \ y \ z]^T$ is the position variable and $\mathbf{p}_o = [x_o \ y_o \ z_o]^T$ is either a constant or a time-varying vector in \mathbb{R}^3 . Assume that $\Upsilon(\mathbf{p}; \mathbf{p}_o)$ has continuous first-order derivatives and increases monotonically with respect to $\|\mathbf{p} - \mathbf{p}_o\|$. Moreover, the level curves of $\Upsilon(\mathbf{p}; \mathbf{p}_o)$, that is, $\Upsilon(\mathbf{p}; \mathbf{p}_o) = \bar{c}$ (where \bar{c} is a positive constant) can enclose a convex region. Then, we utilize the equation $\Upsilon(\mathbf{p}; \mathbf{p}_o) = 1$ to describe the surface of the obstacle, whose center is located at \mathbf{p}_o . For instance, the surface $\Upsilon(\mathbf{p}; \mathbf{p}_o) = \frac{(x-x_o)^2}{a^2} + \frac{(y-y_o)^2}{b^2} + \frac{(z-z_o)^2}{c^2} = 1$ represents an ellipsoid centered at (x_o, y_o, z_o) with axis lengths a, b, c . The obstacle can be static or moving, which depends on the motion of \mathbf{p}_o . Thus, with the help of $\Upsilon(\mathbf{p}; \mathbf{p}_o)$, we can divide the space into three areas: obstacle area \mathcal{A}_o , reactive area \mathcal{A}_r , free area \mathcal{A}_f , which are respectively defined below.

$$\mathcal{A}_o = \{\mathbf{p} \in \mathbb{R}^3 : \Upsilon(\mathbf{p}; \mathbf{p}_o) < 1\}, \quad (44)$$

$$\mathcal{A}_r = \{\mathbf{p} \in \mathbb{R}^3 : 1 \leq \Upsilon(\mathbf{p}; \mathbf{p}_o) \leq \bar{c}\}, \quad (45)$$

$$\mathcal{A}_f = \{\mathbf{p} \in \mathbb{R}^3 : \Upsilon(\mathbf{p}; \mathbf{p}_o) > \bar{c}\}. \quad (46)$$

The obstacle area \mathcal{A}_o is the region where the obstacle occupies, and collision occurs if the nonholonomic robot enters \mathcal{A}_o . Once in the reactive area \mathcal{A}_r , the nonholonomic robot can sense the obstacle and needs to be reactive to the obstacle such that a potential collision can be avoided. Note that the size of the reactive area \mathcal{A}_r can be controlled by the constant \bar{c} . The nonholonomic robot would not be affected by the obstacle when moving in the free area \mathcal{A}_f .

Assumption 1. *The nonholonomic robot's target position \mathbf{p}_d satisfies $\mathbf{p}_d \in \mathcal{A}_f$.*

To design the obstacle avoidance VF (OA-VF), we firstly compute the normal vector at each point on the surface $\Upsilon(\mathbf{p}; \mathbf{p}_o) = k$ ($1 \leq k \leq \bar{c}$), which is given by

$$\mathbf{n}_\Upsilon = \frac{\partial \Upsilon}{\partial x} \mathbf{e}_x + \frac{\partial \Upsilon}{\partial y} \mathbf{e}_y + \frac{\partial \Upsilon}{\partial z} \mathbf{e}_z. \quad (47)$$

The time derivative of \mathbf{n}_Υ is

$$\dot{\mathbf{n}}_\Upsilon = \frac{\partial \mathbf{n}_\Upsilon}{\partial \mathbf{p}} \dot{\mathbf{p}} + \frac{\partial \mathbf{n}_\Upsilon}{\partial \mathbf{p}_o} \dot{\mathbf{p}}_o.$$

For the static obstacles, there holds $\dot{\mathbf{p}}_o = \mathbf{0}$ and the time derivative of \mathbf{n}_Υ degenerates to $\dot{\mathbf{n}}_\Upsilon = \frac{\partial \mathbf{n}_\Upsilon}{\partial \mathbf{p}} \dot{\mathbf{p}}$. Then, based on the normal vector \mathbf{n}_Υ , we propose the OA-VF according to two different cases, which are classified by whether the normal vector \mathbf{n}_Υ is collinear with the N-VF \mathbf{F} given in (3). In the following, we assume the target point \mathbf{p}_d is the origin of the earth-fixed frame \mathcal{F}_e for simplicity.

1) \mathbf{n}_Υ and \mathbf{F} are not collinear ($\mathbf{n}_\Upsilon \nparallel \mathbf{F}$)

Define a new vector τ_Υ^a by the following cross product

$$\tau_\Upsilon^a = \mathbf{n}_\Upsilon \times \mathbf{F}. \quad (48)$$

Substituting (3) and (47) into (48), we obtain that

$$\tau_\Upsilon^a = T_x^a \mathbf{e}_x + T_y^a \mathbf{e}_y + T_z^a \mathbf{e}_z, \quad (49)$$

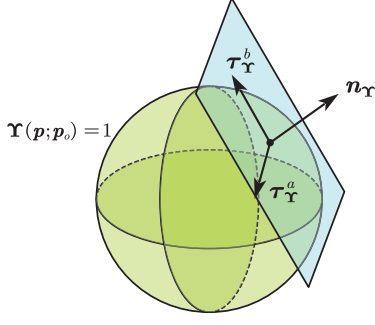


Fig. 3. Vector fields on the obstacle surface.

where the components T_x^a, T_y^a, T_z^a are

$$\begin{aligned} T_x^a &= \frac{\partial \Upsilon}{\partial y} F_z - \frac{\partial \Upsilon}{\partial z} F_y, \\ T_y^a &= \frac{\partial \Upsilon}{\partial z} F_x - \frac{\partial \Upsilon}{\partial x} F_z, \\ T_z^a &= \frac{\partial \Upsilon}{\partial x} F_y - \frac{\partial \Upsilon}{\partial y} F_x. \end{aligned}$$

Then, we define another vector τ_Y^b as follows

$$\tau_Y^b = \tau_Y^a \times \mathbf{n}_Y. \quad (50)$$

By substituting (47) and (48) into (50), it is obtained that

$$\tau_Y^b = T_x^b \mathbf{e}_x + T_y^b \mathbf{e}_y + T_z^b \mathbf{e}_z, \quad (51)$$

where the components T_x^b, T_y^b, T_z^b are

$$\begin{aligned} T_x^b &= \left(\left(\frac{\partial \Upsilon}{\partial z} \right)^2 + \left(\frac{\partial \Upsilon}{\partial y} \right)^2 \right) F_x - \frac{\partial \Upsilon}{\partial x} \left(\frac{\partial \Upsilon}{\partial z} F_z + \frac{\partial \Upsilon}{\partial y} F_y \right), \\ T_y^b &= \left(\left(\frac{\partial \Upsilon}{\partial x} \right)^2 + \left(\frac{\partial \Upsilon}{\partial z} \right)^2 \right) F_y - \frac{\partial \Upsilon}{\partial y} \left(\frac{\partial \Upsilon}{\partial x} F_x + \frac{\partial \Upsilon}{\partial z} F_z \right), \\ T_z^b &= \left(\left(\frac{\partial \Upsilon}{\partial y} \right)^2 + \left(\frac{\partial \Upsilon}{\partial x} \right)^2 \right) F_z - \frac{\partial \Upsilon}{\partial z} \left(\frac{\partial \Upsilon}{\partial y} F_y + \frac{\partial \Upsilon}{\partial x} F_x \right). \end{aligned}$$

2) \mathbf{n}_Y and \mathbf{F} are collinear ($\mathbf{n}_Y \parallel \mathbf{F}$)

When \mathbf{n}_Y and \mathbf{F} are lying in the same straight line, the VF τ_Y^a is undefined since the cross product in (48) is $\mathbf{0}$. In this case, we directly define

$$\tau_Y^a = \mathbf{H}, \quad (52)$$

$$\tau_Y^b = \mathbf{G}, \quad (53)$$

where \mathbf{G} and \mathbf{H} are VFs given in (26) and (32).

Fig. 3 intuitively depicts the VFs $\mathbf{n}_Y, \tau_Y^a, \tau_Y^b$ on the obstacle surface $\Upsilon(\mathbf{p}; \mathbf{p}_o) = 1$. From the geometrical point of view, \mathbf{n}_Y is the normal vector of the obstacle surface, while τ_Y^a and τ_Y^b are the tangential vectors lying in the plane which is orthogonal to \mathbf{n}_Y . Moreover, τ_Y^a and τ_Y^b are also orthogonal to each other. Thus, based on the N-VF \mathbf{F} and the tangential VF τ_Y^b , we propose the OA-VF in the reactive area \mathcal{A}_r as follows

$$\mathbf{F}_{OA} = \chi \mathbf{F} + (1 - \chi) \tau_Y^b, \quad (54)$$

where χ is a smooth function defined by

$$\chi = \begin{cases} 0, & \mathbf{p} \in \{\Upsilon(\mathbf{p}; \mathbf{p}_o) = 1\} \\ S(\mathbf{p}), & \mathbf{p} \in \{1 < \Upsilon(\mathbf{p}; \mathbf{p}_o) < \bar{c}\} \\ 1, & \mathbf{p} \in \{\Upsilon(\mathbf{p}; \mathbf{p}_o) = \bar{c}\} \end{cases} \quad (55)$$

and $S(\mathbf{p})$ is a smooth function valued in $(0, 1)$, which can be constructed by the typical bump functions [41]. The primary requirement for \mathbf{F}_{OA} is to guarantee the obstacle avoidance. Besides, since \mathbf{F}_{OA} is a composite VF of \mathbf{F} and τ_Y^b , we should first investigate whether \mathbf{F}_{OA} has singular points where the nonholonomic robot would get stuck possibly.

Theorem 3. *The OA-VF \mathbf{F}_{OA} proposed in (54) has the following properties:*

- 1) \mathbf{F}_{OA} never penetrates the obstacle area \mathcal{A}_o ;
- 2) \mathbf{F}_{OA} does not vanish in the reactive area \mathcal{A}_r .

Proof. 1) Impenetrability of the obstacle area \mathcal{A}_o can be guaranteed if the OA-VF \mathbf{F}_{OA} projects zero onto the normal vector \mathbf{n}_Y of the obstacle surface $\Upsilon(\mathbf{p}; \mathbf{p}_o) = 1$. In light of this fact, we should compute the dot product of \mathbf{F}_{OA} and \mathbf{n}_Y . According to (54), the OA-VF \mathbf{F}_{OA} on the obstacle surface $\Upsilon(\mathbf{p}; \mathbf{p}_o) = 1$ is equivalent to $\mathbf{F}_{OA}|_{\Upsilon=1} = \tau_Y^b$. Then, it follows that

$$(\mathbf{F}_{OA} \cdot \mathbf{n}_Y)|_{\Upsilon=1} = \tau_Y^b \cdot \mathbf{n}_Y. \quad (56)$$

For the case of $\mathbf{n}_Y \not\parallel \mathbf{F}$, we substitute (50) into (56), and it is obtained that

$$(\mathbf{F}_{OA} \cdot \mathbf{n}_Y)|_{\Upsilon=1} = (\tau_Y^a \times \mathbf{n}_Y) \cdot \mathbf{n}_Y = -(\mathbf{n}_Y \times \mathbf{n}_Y) \cdot \tau_Y^a = 0, \quad (57)$$

where the property of mixed product is utilized. For the case of $\mathbf{n}_Y \parallel \mathbf{F}$, we have

$$(\mathbf{F}_{OA} \cdot \mathbf{n}_Y)|_{\Upsilon=1} = \tau_Y^b \cdot \mathbf{n}_Y = \mathbf{G} \cdot \mathbf{n}_Y, \quad (58)$$

where (53) is employed. Due to $\mathbf{n}_Y \parallel \mathbf{F}$, the normal vector \mathbf{n}_Y can be expressed as $\mathbf{n}_Y = k\mathbf{F}$, where k is a nonzero scalar. By substitute it into (58), we have

$$(\mathbf{F}_{OA} \cdot \mathbf{n}_Y)|_{\Upsilon=1} = k\mathbf{G} \cdot \mathbf{F} = 0, \quad (59)$$

which is guaranteed by (31). Equations (57) and (59) indicate that the OA-VF \mathbf{F}_{OA} is orthogonal to the normal vector \mathbf{n}_Y on the obstacle surface. In other words, the \mathbf{F}_{OA} lies in the tangential plane of the obstacle surface, so that it will never penetrate the obstacle area \mathcal{A}_o .

2) We first consider the case of $\mathbf{n}_Y \not\parallel \mathbf{F}$. For simplicity, we use the components to represent the VFs \mathbf{n}_Y and \mathbf{F} in the following. To be more specific, they are denoted by $\mathbf{n}_Y = [\frac{\partial \Upsilon}{\partial x} \ \frac{\partial \Upsilon}{\partial y} \ \frac{\partial \Upsilon}{\partial z}]^T$ and $\mathbf{F} = [F_x \ F_y \ F_z]^T$, respectively. Under such a formulation, the cross product “ \times ” can be expressed as the hat map “ \wedge ” given in (1). Then, τ_Y^a in (48) can be rewritten as $\tau_Y^a = \mathbf{n}_Y^\wedge \mathbf{F}$, and τ_Y^b in (50) can be rewritten as

$$\tau_Y^b = (\mathbf{n}_Y^\wedge \mathbf{F}) \times \mathbf{n}_Y = -\mathbf{n}_Y^\wedge (\mathbf{n}_Y^\wedge \mathbf{F}) = -(\mathbf{n}_Y^\wedge)^2 \mathbf{F}. \quad (60)$$

By substituting (60) into (54), \mathbf{F}_{OA} can be reorganized as

$$\mathbf{F}_{OA} = \chi \mathbf{F} + (\chi - 1) (\mathbf{n}_Y^\wedge)^2 \mathbf{F} = \Xi_{OA} \mathbf{F}, \quad (61)$$

where Ξ_{OA} is a matrix defined by

$$\Xi_{OA} = \chi \mathbf{I} + (\chi - 1) (\mathbf{n}_Y^\wedge)^2, \quad (62)$$

and \mathbf{I} is the identity matrix. Based on the formulations given in (4), \mathbf{F} only vanishes as the desired point \mathbf{p}_d . According to Assumption 1, there does not exist \mathbf{p}_d in the reactive area

\mathcal{A}_r , implying that $\mathbf{F} \neq \mathbf{0}$ in \mathcal{A}_r . Therefore, referring to (61), \mathbf{F}_{OA} does not vanish in \mathcal{A}_r if and only if the matrix Ξ_{OA} is invertible. By calculation, the determinant of Ξ_{OA} is

$$\det(\Xi_{OA}) = \chi + 2\chi^2(1-\chi)\|\mathbf{n}_\Upsilon\|^2 + \chi(1-\chi)^2\|\mathbf{n}_\Upsilon\|^4. \quad (63)$$

Due to $\|\mathbf{n}_\Upsilon\| \neq 0$, it is obvious that $\det(\Xi_{OA}) \neq 0$ for $0 < \chi \leq 1$, indicating that the matrix Ξ_{OA} is invertible in $\mathcal{A}_r/\{\Upsilon(\mathbf{p}; \mathbf{p}_o) = 1\}$. Once $\mathbf{p} \in \{\Upsilon(\mathbf{p}; \mathbf{p}_o) = 1\}$, i.e., $\chi = 0$, there hold $\det(\Xi_{OA}) = 0$, implying the matrix Ξ_{OA} will lose rank. In this case, \mathbf{F}_{OA} does not vanish if and only if \mathbf{F} does not lie in $\ker(\Xi_{OA})$, which denotes the kernel space of Ξ_{OA} . When $\chi = 0$, Ξ_{OA} degenerates to

$$\Xi_{OA} = -(\mathbf{n}_\Upsilon^\wedge)^2. \quad (64)$$

Thus, it can be derived that

$$\ker(\Xi_{OA}) = \ker(\mathbf{n}_\Upsilon^\wedge) = \{\boldsymbol{\alpha} \in \mathbb{R}^3 : \boldsymbol{\alpha} \parallel \mathbf{n}_\Upsilon\}. \quad (65)$$

Note that the premise of this case is $\mathbf{n}_\Upsilon \nparallel \mathbf{F}$, so that $\mathbf{F} \notin \ker(\Xi_{OA})$ indicating that $\mathbf{F}_{OA} \neq \mathbf{0}$ on the obstacle surface $\Upsilon(\mathbf{p}; \mathbf{p}_o) = 1$. Therefore, \mathbf{F}_{OA} does not vanish in the reactive area \mathcal{A}_r for the case of $\mathbf{n}_\Upsilon \nparallel \mathbf{F}$.

Next, we deal with the case of $\mathbf{n}_\Upsilon \parallel \mathbf{F}$. In this case, owing to the formulation of τ_Υ^b in (53), \mathbf{F}_{OA} in (54) degenerates to

$$\mathbf{F}_{OA} = \chi\mathbf{F} + (1-\chi)\mathbf{G}. \quad (66)$$

According to Lemma 1, the VFs \mathbf{F} and \mathbf{G} are linearly independent. Hence, as the linear combination of \mathbf{F} and \mathbf{G} , the OA-VF \mathbf{F}_{OA} does not vanish everywhere in the reactive area \mathcal{A}_r . \square

Based on Theorem 3, in order to avoid obstacles, the OA-VF \mathbf{F}_{OA} can be employed as the nonholonomic robot's heading direction (i.e., the x -axis direction of the body-fixed frame) in the reactive area \mathcal{A}_r . However, as shown in the free-space motion planning, it is necessary to design another two vector fields to determine the y -axis and z -axis directions of the body-fixed frame \mathcal{F}_e , and the requirement for these three VFs is that each two of them should be orthogonal. The following lemma gives the formulation of the other two VFs.

Lemma 4. Define two VFs \mathbf{G}_{OA} and \mathbf{F}_{OA} by

$$\mathbf{G}_{OA} = \mu\mathbf{G} + (1-\mu)\mathbf{n}_\Upsilon, \quad (67)$$

$$\begin{aligned} \mathbf{H}_{OA} &= \chi\mu\mathbf{H} + (1-\chi)(1-\mu)\tau_\Upsilon^a + \mu(1-\chi)\mathbf{G} \times \tau_\Upsilon^b \\ &\quad + \chi(1-\mu)\mathbf{n}_\Upsilon \times \mathbf{F}, \end{aligned} \quad (68)$$

where μ is given by

$$\mu = \frac{\chi\mathbf{F} \cdot \mathbf{n}_\Upsilon}{\chi\mathbf{F} \cdot \mathbf{n}_\Upsilon + (\chi-1)\tau_\Upsilon^b \cdot \mathbf{G}}, \quad (69)$$

$\mathbf{G}, \mathbf{H}, \mathbf{n}_\Upsilon, \tau_\Upsilon^a, \chi$ are given in (26), (32), (47), (48), (55), respectively. Then, each two VFs of $\mathbf{F}_{OA}, \mathbf{G}_{OA}, \mathbf{H}_{OA}$ are orthogonal.

Proof. We compute the inner product of \mathbf{F}_{OA} and \mathbf{G}_{OA} as given below

$$\begin{aligned} \mathbf{F}_{OA} \cdot \mathbf{G}_{OA} &= \chi\mu\mathbf{F} \cdot \mathbf{G} + (1-\chi)(1-\mu)\tau_\Upsilon^b \cdot \mathbf{n}_\Upsilon \\ &\quad + \chi(1-\mu)\mathbf{F} \cdot \mathbf{n}_\Upsilon + \mu(1-\chi)\tau_\Upsilon^b \cdot \mathbf{G} \end{aligned}$$

Due to $\mathbf{F} \cdot \mathbf{G} = 0$ and $\tau_\Upsilon^b \cdot \mathbf{n}_\Upsilon = 0$, the formulation of $\mathbf{F}_{OA} \cdot \mathbf{G}_{OA}$ can be reorganized as

$$\mathbf{F}_{OA} \cdot \mathbf{G}_{OA} = -\chi\mu(\mathbf{F} \cdot \mathbf{n}_\Upsilon + \frac{\chi-1}{\chi}\tau_\Upsilon^b \cdot \mathbf{G}) + \chi\mathbf{F} \cdot \mathbf{n}_\Upsilon. \quad (70)$$

By substituting (69) into (70), we have $\mathbf{F}_{OA} \cdot \mathbf{G}_{OA} = 0$, indicating that the vector fields \mathbf{F}_{OA} and \mathbf{G}_{OA} are orthogonal.

Next, we compute the cross product of \mathbf{G}_{OA} and \mathbf{F}_{OA} .

$$\begin{aligned} \mathbf{G}_{OA} \times \mathbf{F}_{OA} &= \chi\mu\mathbf{G} \times \mathbf{F} + (1-\chi)(1-\mu)\mathbf{n}_\Upsilon \times \tau_\Upsilon^b \\ &\quad + \mu(1-\chi)\mathbf{G} \times \tau_\Upsilon^b + \chi(1-\mu)\mathbf{n}_\Upsilon \times \mathbf{F}. \end{aligned}$$

Owing to $\mathbf{G} \times \mathbf{F} = \mathbf{H}$ and $\mathbf{n}_\Upsilon \times \tau_\Upsilon^b = \tau_\Upsilon^a$, the formulation of $\mathbf{G}_{OA} \times \mathbf{F}_{OA}$ can be further simplified to be (68), that is, $\mathbf{H}_{OA} = \mathbf{G}_{OA} \times \mathbf{F}_{OA}$, implying that \mathbf{H}_{OA} is orthogonal to \mathbf{F}_{OA} and \mathbf{G}_{OA} , respectively. \square

With the help of Lemma 4, we are able to construct an auxiliary attitude matrix \mathbf{R}_a according to the VFs $\mathbf{F}_{OA}, \mathbf{G}_{OA}, \mathbf{H}_{OA}$. To be more specific, by replacing the components of $\mathbf{F}, \mathbf{G}, \mathbf{H}$ in (35) with those of $\mathbf{F}_{OA}, \mathbf{G}_{OA}, \mathbf{H}_{OA}$, we can obtain an attitude matrix \mathbf{R}_a for obstacle avoidance. Then, based on \mathbf{R}_a , the attitude tracking control input can be designed as (37).

Although the OA-VF \mathbf{F}_{OA} (54) is proposed for one obstacle, it can be easily extended to the situation of multiple obstacles. Assume there exist M obstacles in the workspace and each one can be described by $\Upsilon_i(\mathbf{p}; \mathbf{p}_{oi}) = 1, i = 1, \dots, M$. Then, the obstacle avoidance vector field can be specified as

$$\mathbf{F}_{OA} = \left(\prod_{i=1}^M \chi_i \right) \mathbf{F} + \sum_{i=1}^M ((1-\chi_i)\tau_{\Upsilon_i}^b), \quad (71)$$

where χ_i is the transition function of the i th obstacle, \mathbf{F} is the N-VF of the nonholonomic robot, and $\tau_{\Upsilon_i}^b$ is the tangential VF of the i th obstacle as designed in (50) and (53).

V. COOPERATIVE MOTION PLANNING

This section investigates the cooperative motion planning of multiple nonholonomic robots via VFs, where the main problem is how to achieve collision avoidance among nonholonomic robots. Motivated by the obstacle avoidance results in the previous section, we regard other nonholonomic robots to be avoided as moving obstacles, and introduce different priorities of the nonholonomic robots to deal with the challenge of motion coupling.

Consider a swarm of nonholonomic robots labelled by $\mathcal{V} = \{1, \dots, N\}$ and assume that the dangerous area \mathcal{C}_{ai} of the i -th nonholonomic robot ($i \in \mathcal{V}$) is a sphere given by

$$\mathcal{C}_{ai} = \{\mathbf{p} \in \mathbb{R}^3 : \Psi_i(\mathbf{p}; \mathbf{p}_i) = \|\mathbf{p} - \mathbf{p}_i\| < r_c\}, \quad (72)$$

where \mathbf{p}_i is the position of the i -th nonholonomic robot and r_c is the radius of the sphere. If the dangerous area \mathcal{C}_{ai} is entered by other nonholonomic robots, a potential collision is supposed to occur. Similarly, we can define the reactive area \mathcal{C}_{ri} of the i -th nonholonomic robot by

$$\mathcal{C}_{ri} = \{\mathbf{p} \in \mathbb{R}^3 : r_c \leq \Psi_i(\mathbf{p}; \mathbf{p}_i) \leq r_d\}, \quad (73)$$

where r_d is the communication or detection range of the nonholonomic robot. Thus, the nonholonomic robot should

take actions to avoid collisions once it enters the reactive area \mathcal{C}_{ri} of other nonholonomic robots. The free space \mathcal{C}_{fi} is given by

$$\mathcal{C}_{fi} = \{\mathbf{p} \in \mathbb{R}^3 : \Psi_i(\mathbf{p}; \mathbf{p}_i) > r_d\}, \quad (74)$$

where there is no collision among nonholonomic robots.

Compared to (44)-(46), the above setting of collision avoidance can be regarded as avoiding moving obstacles with sphere boundaries. However, the motion couplings among nonholonomic robots make the collision avoidance essentially different from the obstacle avoidance. To be more specific, the movement of the obstacle is independent of the nonholonomic robot, while in the collision avoidance, the motion of nonholonomic robots relies on each other indeed. Let us take two nonholonomic robots labelled as A and B for example. Once A enters the reactive area of B , it would intend to circumvent B for non-collision. In the meantime, B has also detected A and would take actions to avoid A as well. Such a motion coupling introduces an algebraic loop in mathematics. Thus, compared with obstacle avoidance, how to realize motion decoupling is the main challenge in collision avoidance of multiple nonholonomic robots.

In this paper, we specify a particular priority for each nonholonomic robot to deal with the motion coupling. Specifically, nonholonomic robots are labelled by $i \in \mathcal{V} = \{1, \dots, N\}$, and it is prescribed that the nonholonomic robot with a smaller index has higher priority. That is to say, the 1-st nonholonomic robot possesses the highest priority, while the N -th is the lowest prioritized. Regarding the i -th nonholonomic robot, we define the neighboring label set

$$\mathcal{N}_i = \{j \in \mathcal{V} : \mathbf{p}_i \in \mathcal{C}_{rj}, i \neq j\}. \quad (75)$$

The elements in \mathcal{N}_i are the labels of the nonholonomic robots whose reactive area is entered by the i -th nonholonomic robot. In other words, the nonholonomic robots detected by i -th are collected in \mathcal{N}_i . Next, we select certain labels in \mathcal{N}_i to define another set

$$\mathcal{N}_i^+ = \{j \in \mathcal{N}_i : j < i\}, \quad (76)$$

which collects the nonholonomic robots that are detected by the i -th robot and have higher priorities than the i -th robot. Then, in order to realize collision avoidance, we let the i -th nonholonomic robot avoid the nonholonomic robots in \mathcal{N}_i^+ , while ignore those in $\mathcal{N}_i/\mathcal{N}_i^+$. In this way, the motion of the high prioritized nonholonomic robots is independent from the low prioritized ones, so that the problem of collision avoidance among robots can be converted into the problem of moving obstacles avoidance.

For example, as shown in Fig. 4, there are four nonholonomic robots in the workspace, and the sets \mathcal{N}_i and \mathcal{N}_i^+ ($i \in \mathcal{V} = \{1, 2, 3, 4\}$) can be obtained as

$$\begin{aligned} \mathcal{N}_1 &= \{2, 3, 4\}, & \mathcal{N}_1^+ &= \emptyset, \\ \mathcal{N}_2 &= \{1, 3\}, & \mathcal{N}_2^+ &= \{1\}, \\ \mathcal{N}_3 &= \{1, 2, 4\}, & \mathcal{N}_3^+ &= \{1, 2\}, \\ \mathcal{N}_4 &= \{1, 3\}, & \mathcal{N}_4^+ &= \{1, 3\}. \end{aligned}$$

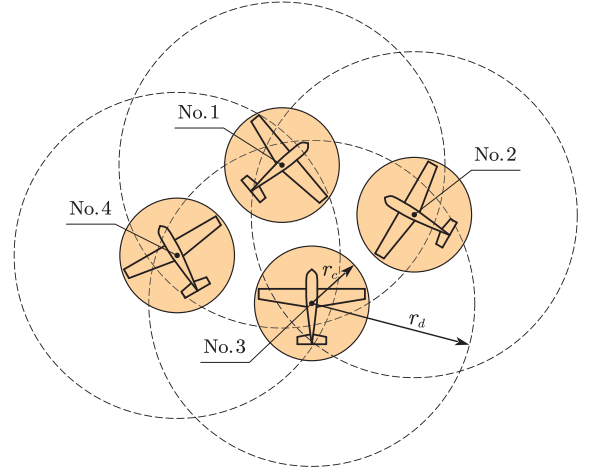


Fig. 4. Collision avoidance of multiple nonholonomic robots (taking fixed-wing UAVs for example).

Then, the labels in \mathcal{N}_i^+ are the nonholonomic robots that the i -th nonholonomic robot should circumvent, by regarding them as independent moving obstacles.

Therefore, similar to (47), we derive the normal vector of the sphere $\Psi_j(\mathbf{p}; \mathbf{p}_j) = \bar{k}$ ($r_c \leq \bar{k} \leq r_d$) as follows

$$\mathbf{n}_{\Psi_j} = \frac{\partial \Psi_j}{\partial x} \mathbf{e}_x + \frac{\partial \Psi_j}{\partial y} \mathbf{e}_y + \frac{\partial \Psi_j}{\partial z} \mathbf{e}_z, \quad (77)$$

and the time derivative of \mathbf{n}_{Ψ_j} is

$$\dot{\mathbf{n}}_{\Psi_j} = \frac{\partial \mathbf{n}_{\Psi_j}}{\partial \mathbf{p}} \dot{\mathbf{p}} + \frac{\partial \mathbf{n}_{\Psi_j}}{\partial \mathbf{p}_j} \dot{\mathbf{p}}_j,$$

where $j \in \mathcal{N}_i^+$. Then, the collision avoidance VF (CA-VF) for the i -th nonholonomic robot can be designed by

$$\mathbf{F}_{CAi} = \left(\prod_{j \in \mathcal{N}_i^+} \chi_j \right) \mathbf{F}_i + \sum_{j \in \mathcal{N}_i^+} ((1 - \chi_j) \boldsymbol{\tau}_{\Psi_j}^b), \quad (78)$$

where \mathbf{F}_i is the N-VF of the i -th nonholonomic robot in the free space, $\boldsymbol{\tau}_{\Psi_j}^b$ is the tangential VF given by

$$\boldsymbol{\tau}_{\Psi_j}^b = \begin{cases} (\mathbf{n}_{\Psi_j} \times \mathbf{F}_i) \times \mathbf{n}_{\Psi_j}, & \text{if } \mathbf{n}_{\Psi_j} \not\parallel \mathbf{F}_i, \\ \mathbf{G}_i, & \text{if } \mathbf{n}_{\Psi_j} \parallel \mathbf{F}_i, \end{cases} \quad (79)$$

and χ_j is the transition function given by

$$\chi_j = \begin{cases} 0, & \mathbf{p} \in \{\Psi_j(\mathbf{p}; \mathbf{p}_j) = r_c\}, \\ S(\mathbf{p}), & \mathbf{p} \in \{r_c < \Psi_j(\mathbf{p}; \mathbf{p}_j) < r_d\}, \\ 1, & \mathbf{p} \in \{\Psi_j(\mathbf{p}; \mathbf{p}_j) = r_d\}. \end{cases} \quad (80)$$

Algorithm 1 summarizes the main procedure to design the CA-VF \mathbf{F}_{CAi} of the i -th nonholonomic robot.

Having designed \mathbf{F}_{CAi} , we can simply construct the auxiliary VFs \mathbf{G}_{CAi} and \mathbf{H}_{CAi} as in Lemma 4. Subsequently, based on \mathbf{F}_{CAi} , \mathbf{G}_{CAi} , \mathbf{H}_{CAi} , the auxiliary attitude matrix \mathbf{R}_a can be constructed as (35), and then the attitude tracking control input Ω^\wedge can be designed accordingly by Lemma 3.

Algorithm 1: Design of the CA-VF F_{CAi}

Input: p_i (the present position of the i -th robot)
Output: F_{CAi} (the CA-VF of the i -th robot)

- 1 Determine the detection range \mathcal{D}_i of the i -th robot
- 2 Detect other robots' position p_j within \mathcal{D}_i
- 3 **for** each $p_j \in \mathcal{D}_i$ **do**
- 4 **if** $p_i \in \mathcal{C}_{rj}$ **then**
- 5 Add j to the set \mathcal{N}_i
- 6 **if** $j < i$ **then**
- 7 Add j to the set \mathcal{N}_i^+
- 8 **end**
- 9 **end**
- 10 **end**
- 11 **for** each $j \in \mathcal{N}_i^+$ **do**
- 12 Compute the vector field n_{Ψ_j}
- 13 **if** $n_{\Psi_j} \nparallel F_i$ **then**
- 14 $\tau_{\Psi_j}^b = (n_{\Psi_j} \times F_i) \times n_{\Psi_j}$
- 15 **else**
- 16 $\tau_{\Psi_j}^b = G_j$
- 17 **end**
- 18 Compute the transition function χ_j
- 19 **end**
- 20 Compute the CA-VF F_{CAi} as (78)

VI. NUMERICAL SIMULATION RESULTS

In this section, we provide three numerical simulation examples based on fixed-wing UAVs to verify the effectiveness of the proposed motion planning algorithms.

The first example is to drive a fixed-wing UAV to the target position with the desired heading direction in an obstacle-free environment. The target position is chosen as the origin of \mathcal{F}_{xyz} and the desired heading direction is specified as the positive direction of the x -axis. The simulation is carried out based on six initial conditions, including the position and orientation of the fixed-wing UAV. Fig. 5 depicts the trajectories of the fixed-wing UAV from different initial conditions, demonstrating that the fixed-wing UAV reaches the goal point with the specified heading direction. The position and orientation of the fixed-wing UAV evolving with time are shown in Fig. 6, where the orientation is parameterized as the Euler angles for the sake of illustration. Particularly, as seen in Fig. 6, the pitch and yaw angles converge to zero, indicating that the heading direction of the fixed-wing UAV points to the x -axis of \mathcal{F}_{xyz} .

In the second example, the fixed-wing UAV moves in an obstacle-cluttered environment. By following the obstacle description given in [42], the obstacles in this simulation example are formulated by

$$\Upsilon(\mathbf{p}; \mathbf{p}_o) = \left(\frac{x - x_o}{a} \right)^{2p} + \left(\frac{y - y_o}{b} \right)^{2q} + \left(\frac{z - z_o}{c} \right)^{2r} = 1,$$

where p, q, r are used to describe the geometrical shape of the obstacle, and a, b, c are used to control the size of the obstacle. By choosing different p, q, r , the equation $\Upsilon(\mathbf{p}; \mathbf{p}_o) = 1$ represents the ellipsoid, cylinder, cone, etc. Simulation results based on three different initial conditions are given in Fig. 7,

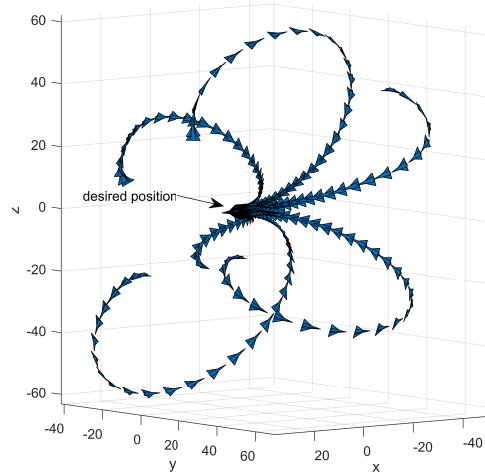


Fig. 5. Trajectories of a fixed-wing UAV moving in an obstacle-free environment (with six different initial conditions).

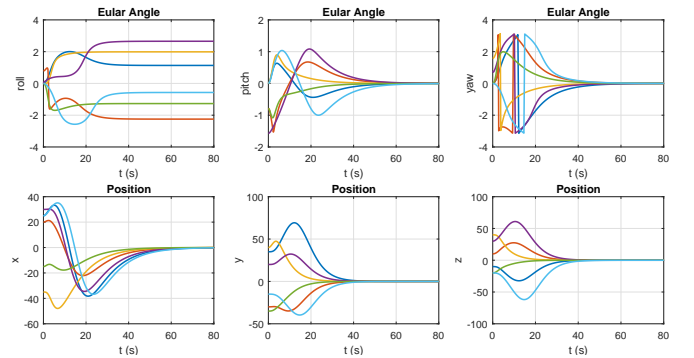


Fig. 6. Position and orientation evolution of the fixed-wing UAV.

where the target position is chosen as $(75, 30, 25)$, and the desired heading direction is specified as the positive direction of the x -axis.

The third example provides the motion planning results of seven fixed-wing UAVs with collision avoidance. As shown in Fig. 8, each fixed-wing UAV is required to reach its desired position and keep the heading direction as the initial time. It can be observed that the fixed-wing UAVs achieve the goal of motion planning and do not collide with each other. Besides, we note that the fixed-wing UAV in the middle of the line (which is marked in dark blue) is labelled by $i = 1$, so that it has the highest priority and its movement is not influenced by others. In contrast, the fixed-wing UAV starting from the position $(0, 0, 0)$ (which is marked in dark magenta) is the lowest prioritized, and thus it has to avoid the rest of all fixed-wing UAVs.

VII. CONCLUSION

This paper has presented a novel velocity vector field for nonholonomic robots in 3D, which can solve the motion planning problem with the requirement of reaching not only target positions but also heading directions. A composite vector field has been further presented to ensure collision avoidance with

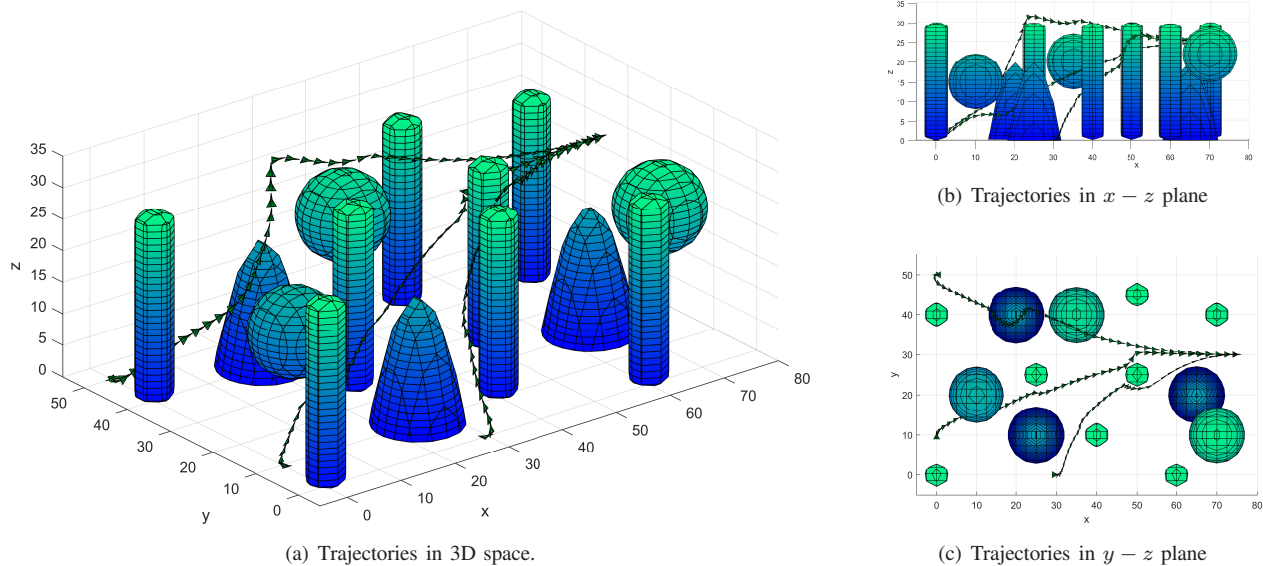


Fig. 7. Trajectories of a fixed-wing UAV moving in an obstacle-cluttered environment (three different initial conditions).

REFERENCES

- [1] J. Wang, M. Q.-H. Meng, and O. Khatib, "EB-RRT: Optimal motion planning for mobile robots," *IEEE Trans. Autom. Sci. Eng.*, vol. 17, no. 4, pp. 2063–2073, Oct. 2020.
- [2] J. Li, M. Ran, and L. Xie, "Efficient trajectory planning for multiple non-holonomic mobile robots via prioritized trajectory optimization," *IEEE Robot. Autom. Lett.*, vol. 6, no. 2, pp. 405–412, Apr. 2021.
- [3] G. Zhao and M. Zhu, "Pareto optimal multirobot motion planning," *IEEE Trans. Autom. Control*, vol. 66, no. 9, pp. 3984–3999, Sep. 2021.
- [4] H. Zhou, Z. Ren, M. Marley, and R. Skjetne, "A guidance and maneuvering control system design with anti-collision using stream functions with vortex flows for autonomous marine vessels," *IEEE Trans. Control Syst. Technol.*, vol. 30, no. 6, pp. 2630–2645, Nov. 2022.
- [5] V. Hassani and S. V. Lande, "Path planning for marine vehicles using Bézier curves," *IFAC-PapersOnLine*, vol. 51, no. 29, pp. 305–310, Oct. 2018.
- [6] M. D. Pedersen and T. I. Fossen, "Marine vessel path planning & guidance using potential flow," *IFAC Proc. Volumes*, vol. 45, no. 27, p. 188–193, 2012.
- [7] B. Zhou, J. Pan, F. Gao, and S. Shen, "Raptor: Robust and perception-aware trajectory replanning for quadrotor fast flight," *IEEE Trans. Robot.*, vol. 37, no. 6, pp. 1992–2009, Dec. 2021.
- [8] X. Zhou, Z. Wang, C. Xu, and F. Gao, "Ego-planner: An ESDF-free gradient-based local planner for quadrotors," *IEEE Robot. Autom. Lett.*, vol. 6, no. 2, pp. 478–485, Apr. 2021.
- [9] J. Tordesillas and J. P. How, "MADER: Trajectory planner in multiagent and dynamic environments," *IEEE Trans. Robot.*, vol. 38, no. 1, pp. 463–476, Feb. 2022.
- [10] X. Wang, L. Shen, Z. Liu, S. Zhao, Y. Cong, Z. Li, S. Jia, H. Chen, Y. Yu, Y. Chang, and Y. Wang, "Coordinated flight control of miniature fixed-wing UAV swarms: methods and experiments," *Sci. China Inf. Sci.*, vol. 62, Nov. 2019, art. no. 212204.
- [11] J. M. Levin, M. Nahon, and A. A. Paranjape, "Real-time motion planning with a fixed-wing UAV using an agile maneuver space," *Auton. Robot.*, vol. 43, no. 8, pp. 2111–2130, Dec. 2019.
- [12] G. Aiello, K. P. Valavanis, and A. Rizzo, "Fixed-wing UAV energy efficient 3D path planning in cluttered environments," *J. Intell. Robot. Syst.*, vol. 105, no. 3, Jul. 2022, art. no. 60.
- [13] S. Fari, X. M. Wang, S. Roy, and S. Baldi, "Addressing unmodeled pathfollowing dynamics via adaptive vector field: A UAV test case," *IEEE Trans. Aerosp. Electron. Syst.*, vol. 56, no. 2, p. 1613–1622, Apr. 2020.
- [14] O. Egeland, M. Dalsmo, and O. J. Sjørdalen, "Feedback control of a nonholonomic underwater vehicle with a constant desired configuration," *Int. J. Robotics Res.*, vol. 15, no. 1, pp. 24–35, Feb. 1996.

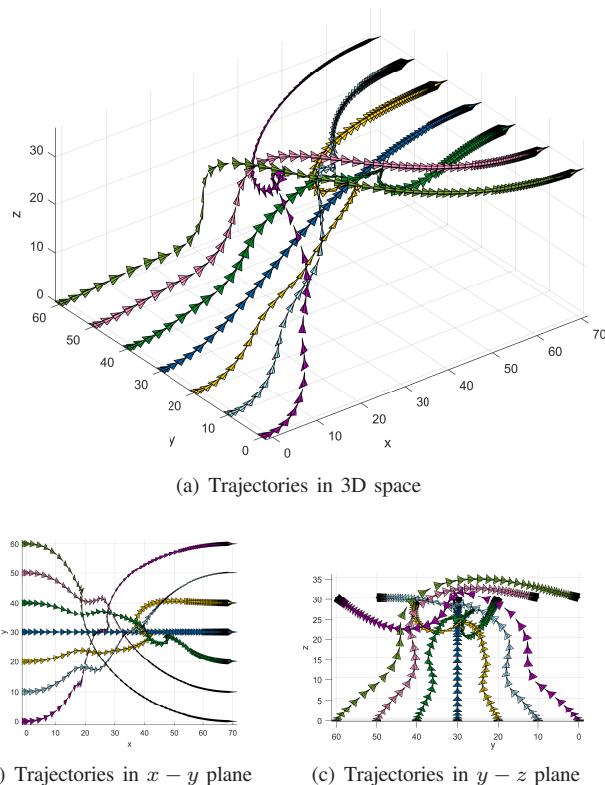


Fig. 8. Trajectories of seven fixed-wing UAVs with collision avoidance.

obstacles and other robots by guaranteeing no penetration of the dangerous area. In addition, we have proposed a priority-based algorithm to achieve motion decoupling among multiple nonholonomic robots. Future research will focus on the motion planning in more practical scenarios, such as input saturation constraints, path curvature constraints, robust motion with measurement noises, and so on.

- [15] S. Li and X. Wang, "Finite-time consensus and collision avoidance control algorithms for multiple AUVs," *Automatica*, vol. 49, no. 11, pp. 3359–3367, Nov. 2013.
- [16] H. P. Li, P. Xie, and W. S. Yan, "Receding horizon formation tracking control of constrained underactuated autonomous underwater vehicles," *IEEE Trans. Ind. Electron.*, vol. 64, no. 6, pp. 5004–5013, Jun. 2017.
- [17] X. He, Z. Sun, Z. Geng, and A. Robertsson, "Exponential set-point stabilization of underactuated vehicles moving in three-dimensional space," *IEEE/CAA J. Autom. Sinica*, vol. 9, no. 2, pp. 270–282, Feb. 2022.
- [18] R. W. Beard and T. W. McLain, *Small Unmanned Aircraft: Theory and Practice*. Princeton, New Jersey: Princeton University Press, 2012.
- [19] L. E. Kavraki, P. Svestka, J. C. Latombe, and M. H. Overmars, "Probabilistic roadmaps for path planning in high-dimensional configuration spaces," *IEEE Trans. Robot. Autom.*, vol. 12, no. 4, pp. 566–580, Aug. 1996.
- [20] P. Bhattacharya and M. L. Gavrilova, "Roadmap-based path planning: Using the voronoi diagram for a clearance-based shortest path," *IEEE Robot. Autom. Mag.*, vol. 15, no. 2, pp. 58–66, Jun. 2008.
- [21] P. Lehner and A. Albu-Schaffer, "The repetition roadmap for repetitive constrained motion planning," *IEEE Robot. Autom. Lett.*, vol. 3, no. 4, pp. 3884–3891, Oct. 2018.
- [22] C. Cai and S. Ferrari, "Information-driven sensor path planning by approximate cell decomposition," *IEEE Trans. Syst., Man, Cybern. B*, vol. 39, no. 3, pp. 672–689, Jun. 2009.
- [23] L. Zhang, Y. J. Kim, and D. Manocha, "Efficient cell labelling and path non-existence computation using c-obstacle query," *Int. J. Robotics Res.*, vol. 27, no. 11-12, pp. 1246–1257, Nov. 2008.
- [24] R. V. Cowlagi and P. Tsiotras, "Multiresolution motion planning for autonomous agents via wavelet-based cell decompositions," *IEEE Trans. Syst., Man, Cybern. B*, vol. 42, no. 5, pp. 1455–1469, Oct. 2012.
- [25] S. Karaman and E. Frazzoli, "Sampling-based algorithms for optimal motion planning," *Int. J. Robotics Res.*, vol. 30, no. 7, pp. 846–894, Jun. 2011.
- [26] L. Jaillet, J. Cortes, and T. Simeon, "Sampling-based path planning on configuration-space costmaps," *IEEE Trans. Robot.*, vol. 26, no. 4, pp. 635–646, Aug. 2010.
- [27] Y. Oh, K. Cho, Y. Choi, and S. Oh, "Chance-constrained multilayered sampling-based path planning for temporal logic-based missions," *IEEE Trans. Autom. Control*, vol. 66, no. 12, pp. 5816–5829, Dec. 2021.
- [28] I. I. Hussein and A. M. Bloch, "Optimal control of underactuated non-holonomic mechanical systems," *IEEE Trans. Autom. Control*, vol. 53, no. 3, pp. 668–682, Apr. 2008.
- [29] A. J. Häusler, A. Saccon, A. P. Aguiar, J. Hauser, and A. M. Pascoal, "Energy-optimal motion planning for multiple robotic vehicles with collision avoidance," *IEEE Trans. Control Syst. Technol.*, vol. 24, no. 3, pp. 867–883, May 2016.
- [30] V. Cichella, I. Kammer, C. Walton, N. Hovakimyan, and A. M. Pascoal, "Optimal multivehicle motion planning using Bernstein approximants," *IEEE Trans. Autom. Control*, vol. 66, no. 4, pp. 1453–1466, Apr. 2021.
- [31] G. Zhao and M. Zhu, "Scalable distributed algorithms for multi-robot near-optimal motion planning," *Automatica*, vol. 140, Jun. 2022, art. no. 110241.
- [32] B. Li, Y. Ouyang, Y. Zhang, T. Acarman, Q. Kong, and Z. Shao, "Optimal cooperative maneuver planning for multiple nonholonomic robots in a tiny environment via adaptive-scaling constrained optimization," *IEEE Robot. Autom. Lett.*, vol. 6, no. 2, pp. 1511–1518, Apr. 2021.
- [33] A. Bloch, M. Camarinha, and L. Colombo, "Dynamic interpolation for obstacle avoidance on Riemannian manifolds," *Int. J. Control*, vol. 94, no. 3, pp. 588–600, Mar. 2021.
- [34] S. R. Lindemann and S. M. LaValle, "Simple and efficient algorithms for computing smooth, collision-free feedback laws over given cell decompositions," *Int. J. Robotics Res.*, vol. 28, no. 5, pp. 600–621, May 2009.
- [35] D. Panagou, "A distributed feedback motion planning protocol for multiple unicycle agents of different classes," *IEEE Trans. Autom. Control*, vol. 62, no. 3, pp. 1178–1193, Mar. 2017.
- [36] A. Marchidan and E. Bakolas, "Collision avoidance for an unmanned aerial vehicle in the presence of static and moving obstacles," *J. Guid. Control Dyn.*, vol. 43, no. 1, pp. 96–110, Jan. 2020.
- [37] Y. A. Kapitanyuk, A. V. Proskurnikov, and M. Cao, "A guiding vector-field algorithm for path-following control of nonholonomic mobile robots," *IEEE Trans. Control Syst. Technol.*, vol. 26, no. 4, pp. 1372–1385, Jul. 2018.
- [38] W. Yao, B. Lin, B. D. O. Anderson, and M. Cao, "Guiding vector fields for following occluded paths," *IEEE Trans. Autom. Control*, vol. 67, no. 8, pp. 4091–4106, Aug. 2022.
- [39] X. He and Z. Li, "Simultaneous position and orientation planning of nonholonomic multi-robot systems: A dynamic vector field approach," 2022, arXiv:2209.00955.
- [40] F. Bullo and R. Murray, "Proportional derivative (PD) control on the Euclidean group," in *Proc. European Control Conference*, Rome, Italy, Sep. 1995, pp. 1091–1097.
- [41] R. Fry and S. McManus, "Smooth bump functions and the geometry of banach spaces: a brief survey," *Expositiones Mathematicae*, vol. 20, no. 2, pp. 143–183, 2002.
- [42] O. Khatib, "Real-time obstacle avoidance for manipulators and mobile robots," *Int. J. Robot. Res.*, vol. 5, no. 1, pp. 90–98, 1986.